Development of novel metal-supported proton ceramic electrolyser cell with thin film BZY15–Ni electrode and BZY15 electrolyte

M. Stange[1*], E. Stefan[2], C. Denonville[1], Y. Larring[1], P. M. Rørvik[1], R. Haugsrud[2]

[1] SINTEF Materials and Chemistry, P.O. Box 124, Blindern, N-0314 Oslo, Norway

[2] Dept. of Chemistry, University of Oslo, FERMIO, Gaustadalleen 21, 0349 Oslo, Norway

* Corresponding author: marit.stange@sintef.no

Abstract

Metal supports for planar MS-PCEC were manufactured using tape-casting of low-cost ferritic stainless steel. A coating protecting the metal support against oxidation was applied by vacuum infiltration and a buffer layer of $La_{0.5}Sr_{0.5}Ti_{0.75}Ni_{0.25}O_{3-\delta}$ (LSTN) was further deposited to smoothen the surface. The $BaZr_{0.85}Y_{0.15}O_{3-\delta}$–NiO (BZY15–NiO) cathode and the $BaZr_{0.85}Y_{0.15}O_{3-\delta}$ (BZY15) electrolyte were applied by pulsed laser deposition (PLD) at elevated substrate temperatures (at 700 °C and 600 °C respectively). The main challenges are related to the restrictions in sintering temperature and atmosphere induced by the metal support, as well as strict demands on the roughness of substrates used for PLD. Reduction treatment of the half cells confirmed that NiO in the BZY15–NiO layer was reduced to Ni, resulting in increased porosity of the BZY15–Ni cathode, while keeping the columnar and dense microstructure of the BZY15 electrolyte. Initial electrochemical testing with a Pt anode showed a total resistance of 40 $\Omega \cdot cm^2$ at 600 °C. Through this work important advances in using metal supports and thin films in planar PCEC assemblies have been made.

Keywords: Protonic ceramic electrolysis cell (PCEC), tape casting, thin film deposition, metal supports

Highlights:

- Tape-casted metal supports (MS) with coatings are developed
- Spray-coated buffer layers suitable for thin films deposited by PLD
- High temperature sintering steps detrimental to the metal supports are eliminated
- Thin films of porous $BaZr_{0.85}Y_{0.15}O_{3-\delta}$–NiO (BZY15–NiO) and dense BZY15 deposited
- Microstructure optimised by deposition at different temperatures and pressures

1. Introduction

Hydrogen production via electrolysis of water has positive environmental impact compared to reforming of fossil fuel without CO_2 capture. The total energy demand of the process drops considerably when water shifts from liquid to gas phase and higher operation temperatures are beneficial.Water electrolysis using proton-exchange membrane (PEM) cells operates at 70–80 °C and requires a large amount of electricity [1,2], making hydrogen production with solid oxide electrolysis cells (SOECs) more viable [3,4], particularly when waste heat from industry or renewables sources (*e.g.*, solar or geo-thermal plants) are utilized as the heat source.

For SOECs based on conventional oxygen-ion conductors, the need to remove water from the produced hydrogen, the low electrode stability, and the high operating temperature (750 to 1000 °C which is higher than that of the waste heat from industries), limit the deployment. Proton ceramic electrolyzer cell (PCEC) alleviates these challenges by producing electrochemically pressurized, dry hydrogen at operating temperatures between 500 and 700 °C, and the dry H_2 produced avoid risk of oxidation of hydrogen electrode (cathode). Introduction of thin film electrodes and proton conducting electrolyte on a metal support (MS-PCEC) enables better thermal conduction (reduced thermal stresses) and the possibility for additional reduction in the operating temperature due to reduced resistance of the thin film functional layers. Lower operation temperatures open up for the use of cheaper materials such as steel-based interconnects and metal-supported electrodes. PCEC further avoids steam corrosion of the metal support and oxidation of the Ni electrode observed for SOECs [5], since the oxygen activity in the produced H_2 (dry) at the metal support is below the stability range of the oxides. Overall, PCEC is favorable for coupling to renewable energies and increased lifetime [6] .

Porous metal supports are expected to have high potential for mobile applications because of their relatively high resistance to thermal and mechanical stress [7]. They also enable the use of well-established joining techniques such as welding and brazing [8]. Metal-supported cells, however, call for low temperature processing routes since the metal alloy can only withstand sintering up to ~1300 °C without partly densification and/or melting. This is not compatible with the processing of high temperature proton conducting ceramics such as barium zirconate-

based materials (*e.g.*, $BaZr_{0.85}Y_{0.15}O_{3-\delta}$ = BZY15), which typically require sintering temperatures ≥ 1500 °C. These restrictions therefore exclude traditional powder based synthesis of BZY15–Ni cermet electrode and BZY15 electrolyte and other processing routes must be developed for the fabrication of MS-PCEC. To the authors knowledge, no reports on MS-PCEC or MS-PCFC have been published.

Fabrication of PCFC with a BZY electrolyte using traditional high temperature routes, shows high ohmic resistance of the electrolyte due to high grain boundary resistance resulting in large ohmic resistance and low power outputs of the cell [9,10]. Recently, highly conductive, grain-boundary free thin-film BZY electrolytes have been fabricated using pulsed laser deposition (PLD) [11,12]. PLD is a versatile method for optimized processing of electrode and electrolyte thin films for fuel cells and electrolyser cells at lower temperatures [11–18]. PLD has for instance been used to deposite thin electrolyte layers on porous YSZ–NiO electrode supports. [19–21]. PLD fabrication has mostly been performed with small samples. However, recently, large-area deposition with PLD became available, in diameter up to 200mm [22]. These systems are used for high-speed deposition of thin films such as piezoelectric $Pb(Zr,Ti)O_3$ (PZT) for micro-electronical–mechanical systems (MEMS) applications, ionic conducting YSZ for fuel cells or transparent electrical conducting layers on sensitive substrates, like flexible displays and OLEDs. PLD has the advantage of stoichiometric transfer and a strong bonding with the substrate of the deposited composition. PLD requires smooth surfaces for successful deposition of thin films.. In a very recent work, a thin nano-crystalline electrode functional layer of BZY–NiO was deposited by PLD on a tape casted layer of BZY–NiO in order to reduce grain size and pore sizes and provide flat surface favorable for BZY electrolyte deposition by PLD[12]. Significantly improved power outputs were obtained from the fuel cell configuration with maximum power density of $740 mW cm^{-2}$ at 600 °C.

As shown in our previous paper, the poor sinterability of BZY15–Ni on the metal support in reducing atmosphere and temperature ~1300 °C hindered the successful deposition of a dense electrolyte film [23]. In the current work it was therefore necessary to develop a smooth conducting buffer layer on the metal support with sintering temperature below 1200 °C. Reported results on $La_{0.5}Sr_{0.5}Ti_{0.75}Ni_{0.25}O_{3-\delta}$ [24] indicate that the material is a good candidate for such intermediary layers between the metal substrate and other thin film cell components

implemented by PLD. Exsolution of metallic Ni nanoparticles during operation was even found to coincide with a dramatic (absolute) drop in the water splitting onset potential [25].

In this work, we present a fabrication procedure for manufacturing of single MS-PCEC cells with a thin electrolyte using scalable and flexible techniques. For the first time, MS-PCEC have been made with a cathode and an electrolyte deposited by PLD as illustrated in Figure 1. The metal substrate is prepared by water-based tape-casting and protective Lanthanum-Manganese-Cobalt coatings are applied to avoid oxidation during cell fabrication and testing using vacuum infiltration [26]. A conducting buffer layer is deposited by spray-coating, while PLD is applied to grow thin layers of BZY15–NiO electrode and BZY15 electrolyte. The manufacturing process enables to decrease the total thickness of the electrolyzer cell and eliminates the need for high temperature sintering steps above 1200 °C which are detrimental to the metal support. The oxidation of coated and uncoated metal supports has been studied by thermogravimetry and compared to elucidate effects of the coating on oxidation kinetics.

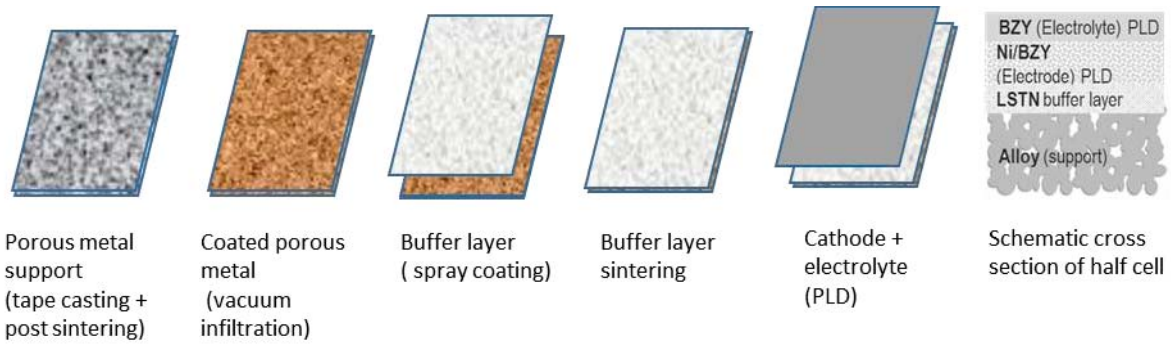

Figure 1. Fabrication procedure for MS-PCEC half cell.

2. Experimental

The fabrication procedure is illustrated in Figure 1. Highly porous and robust metal supports of low cost ferritic stainless steel (20.6%Cr) were prepared using aqueous tape-casting as described in [26]. The particle size distribution of the metallic powder from Höganäs AB, Sweden, was characterised by means of static image analysis with the a Malvern Morphology G3 apparatus.

The green tapes were pre-annealed at temperatures between 1100 and 1300 °C in reducing atmosphere (4% H_2 in Ar) to obtain a support with sufficient mechanical strength for the cathode and electrolyte fabrication steps and at the same time preserve sufficient shrinkage capability to match densification of the buffer layer. A protective coating was applied on the sintered supports by vacuum infiltration of a lanthanum-manganese-cobalt solution with $La(Mn_{0.5}Co_{0.5})_{0.8}$ stoichiometry, followed by fast curing; 30 s at 900 °C in air [26].
A layer of $La_{0.5}Sr_{0.5}Ti_{0.75}Ni_{0.25}O_3$ (LSTN, CerPoTech, Norway) was deposited on the metal support with a SONOTEK spray coater. The final layer should have a defect free surface with roughness below 3 μm and without pores larger than 1 μm to allow the subsequent deposition of the electrolyte by PLD. Several LSTN suspensions, with varing solid content from 22 to 37 wt%, were prepared by dispersing LSTN powder in isopropanol for 1 h before 10 min sonification was applied using a BRANSON sonifier probe. It is essential to prevent extensive infiltration of LSTN powder into the support during spray coating and to smoothen the surface of the spray-coated layer promoting deposition of defect free layers with PLD. The number of spray-coating depositions applied to obtain a 40 μm thick LSTN layer varied from 3 to 7 depending on the content of solid in the suspension and the spray flow rate (varied from 0.25 to 1 mL min^{-1}). In order to fill the largest holes present in the metal support, impossible to cover with spray coating, a LSTN layer was applied on the metal support before spray coating using a concentrated slurry (37.5 wt% solid content) and a squeegee. The assembly (buffer layer on metal support) was sintered in reducing atmosphere (4% H_2 in Ar) at temperatures between 1125 °C to 1225 °C, for 2 h.

$BaZr_{0.85}Y_{0.15}O_{3-\delta}$ (BZY15) and BZY15–NiO ceramic targets used for PLD were prepared from commercial powder (CerPoTech, Norway). Cathode and electrolyte layers (Figure 1) were prepared using a PLD workstation (SURFACE systems+technology GmbH & Co. KG, Germany, with a COMPex *Pro* 205, Coherent, KrF excimer laser, $\lambda = 248$ nm and pulse length of 25 ns). Prior to deposition the chamber was evacuated to 5×10^{-6} mbar. Samples were heated in the temperature range of 600 – 700 °C. The energy density was set to 1.0–1.6 J cm^{-2}, the laser frequency to 5 – 7 Hz, and the target-substrate distance (TSD) was kept constant at 6 cm. Depositions were done at gradually decreasing O_2 pressure of 0.25 – 0.15 mbar for the BZY15–NiO cathode and at 0.1 – 0.02 mbar for the BZY15 electrolyte.

The morphology and chemical composition of powders and cell components were characterized by field emission gun scanning electron microscopy (FEG-SEM) coupled to an

electron dispersive spectrometer (EDS) (SEM Quanta 200 and NovaNano SEM 650 from FEI). The surface roughness of the spray-coated cathods/buffer layers was determined with white light interferometry (WLI) (Wyko NT9800).

X-ray diffraction patterns of PLD films were collected in grazing angle mode (GI-XRD) with parallel beam geometry, on a PANalytical Empyrean X-ray diffractometer (CuKα radiation) equipped with a Proportional detector Xe. The data were collected at an incidence beam angle of $\omega = 1°$, for 2θ from 10° to 120°.

Isothermal oxidation of coated and un-coated metal supports was studied by thermogravimetric analysis (TGA, CI Robal MK1 microbalance) in bottle-dry air and humidified (2.5% H_2O) 5%H_2/Ar at 600, 700 and 800 °C.

In order to observe the reduction of the BZY–NiO to BZY–Ni, two half cell assemblies were annealed at temperatures between 450 – 750 °C under a H_2/Ar atmosphere on the cathode side.

For initial electrochemical measurements, a MS/LSTN/(BZY15–NiO)/BZY15 half cell (diameter 20 mm) was mounted in a Probostat cell (NorECs, Norway) using a 2-point 4-wire setup . Electrical contacts to the cell were made using Pt net and Pt paste; thus, Pt acted as anode (top electrode) in the measurements. The geometric area of the Pt electrode was 0.785 cm^2. The cell was sealed using mica with a small load and therefore not fully gastight, this to avoid mechanical damage of the cell. This sealing was sufficient to obtain an impression of the cell quality. The electrochemical measurements were performed by electrochemical impedance spectroscopy (EIS) in the frequency range 1 MHz – 1 Hz with 100 mV AC perturbation using a Solartron 1287 potensiostat combined with a Solartron 1255B analyzer. The measurements were made at equilibrium, in the temperature range of 450 – 650 °C, under humidified Ar (3% humidity) on the Pt side and dry 0 – 100% H_2 in Ar on the MS side.

3. Results and discussion

The fabrication route of the metal-supported half cell is summarized in Figure 1. In the following the different fabrication steps will be described and discussed, together with the reduction of NiO to Ni in H_2/Ar atmosphere after deposition of PLD layers. The oxidation behaviour of coated and uncoated metal supports in air and humidified 5%H_2/Ar will be summarized in order to assess the durability and corrosion behavior in of the metal supports during fabrication and testing.

Tape casting of metal sheets: Parameters such as the type of alloy powder and pore former particle size distribution and content, the binder/plasticizer ratio, as well as the pre-sintering procedures were all optimized to tailor microstructure and mechanical strength of the metal supports. The mean particle size of the metallic powder was 50 µm, with a broad particle size distribution ranging from 2 to 110 µm. In addition, the characterisation with Malvern Morphology G3 showed that the particle shape is not spherical which influences the particle flow during tape casting and surface roughness after sintering. Pre-sintering temperature of the metal support was investigated to obtain sufficent mechanical strength for cathode and electrolyte deposition. The importance of annealing temperature is illustrated in Figure 2 showing SEM micrographs of metal support sintered at 1100, 1200 and 1300 °C for 2 h in 4%H_2/Ar. Figure 2a) reveals high porosity and lack of neck growth for the lower annealing temperature, explaining why the mechanical strength of these supports was insufficient for further processing. Supports sintered at higher temperatures demonstrated high mechanical strength, nevertheless supports sintered at 1300°C were warped with lower porosity and therefore not suitable. Supports sintered between 1130 – 1200 °C were therefore used for further processing.

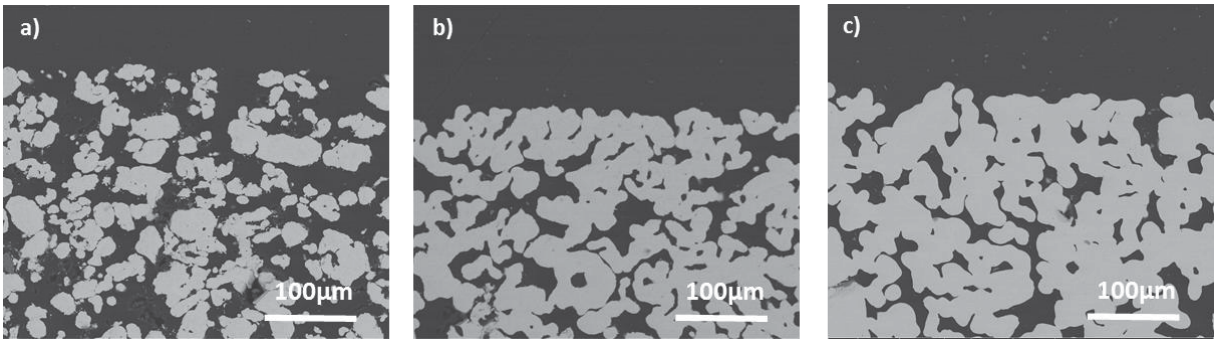

Figure 2 SEM micrographs of metal supports sintered at a) 1100 °C; b) 1200 °C and c) 1300 °C in dry 4% H_2/Ar.

Metal support coating and oxidation testing: The porous metal supports were characterized in SEM before and after applying the protective coating, see Figure 3. Figure 3 (c) shows that the coating wets the metal support. The thickness of the coating is inhomogeneous on the surface of the metal support and is found in excess in the trenches between the metal grains due to capillary effects.

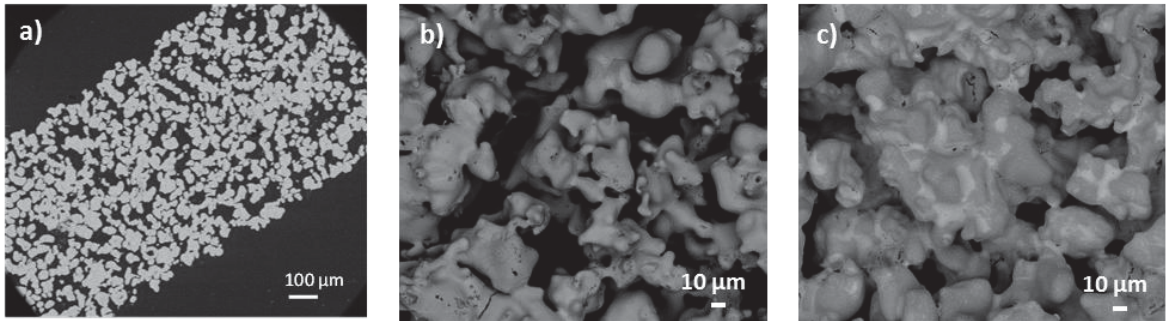

Figure 3 SEM micrographs of a metal support before and after coating; (a) cross section and (b) surface of a metal support after pre-annealing at 1175 °C, and (c) surface of a coated metal support after curing in air.

The oxidation behavior of the coated and uncoated metal support was studied at constant temperatures (600, 700, 800 °C), in air and humidified (2.5% H_2O) 5%H_2/Ar. A summary of the oxidation tests is presented in Figure 4 as a columnar plot of the mass gain upon oxidation. The coating significantly improved the oxidation resistance of the metal supports, both in air and wet H_2/Ar at 600 and 700 °C. At 800 °C the coated metal support showed limited oxidation in wet H_2/Ar. The rather substantial oxidation in air confirms that, even coated, the MS is not suitable for the air side of the MS-PCEC at T > 700°C. Detailed characterization of the corroded samples and corrosion kinetics will be published elsewhere.

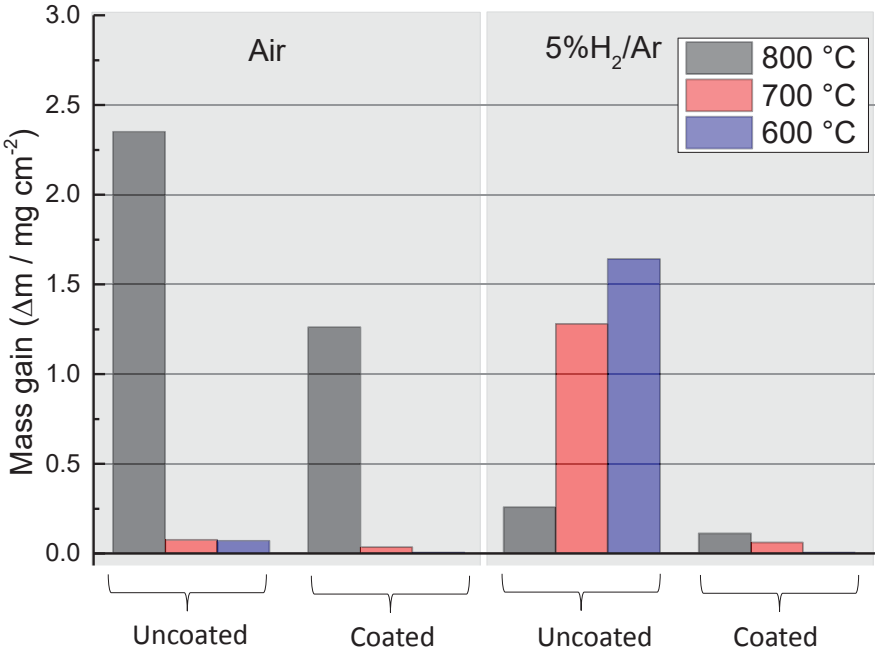

Figure 4 Mass gain upon oxidation of coated and uncoated metal supports in air and wet 5% H_2/Ar at 600, 700, and 800 °C after ≥ 200 h.

Spray coating of buffer layers: A spray-coated layer of LSTN was added to decrease the surface roughness of the metal support and to facilitate formation of continuous films by PLD. After optimizing the metal support pre-annealing temperature; LSTN slurry concentration; spray coating deposition parameters and sintering temperature of the MS/LSTN structures the LSTN layers were without holes and cracks, and had a surface roughness of ~1–3 µm. The progress in the development of MS/LSTN structures is depicted in Figure 5 by some examples of the LSTN layers obtained using spray-coating parameters presented in Table 1. The parameters were adjusted in parallel to the pre-annealing temperature of the metal support and LSTN layer. The ideal sintering temperature range was found to be 1160 – 1175 °C, since the PLD films delaminated from MS/LSTN samples sinterered at lower temperature, while higher sintering temperature resulted in cracks in the LSTN layer due to bending of the metal support which made them unsuitable for PLD. Spray coating using the highly concentrated suspensions (37 wt%, Table 1) were unstable and resulted in pulsed spray and inhomogenous deposition. Decreasing the concentration of the LSTN suspension improved the stability of the deposition but did not allow complete covering of the large pores present in the support. To obtain a thin and smooth defect free layer suitable for PLD, the layer applied with a

squeegee was necessary. Two surface profiles of LSTN spray-coated layers after sintering, characterised by white light interferometry (WLI), are presented in Figure 6 to illustrate a) sharp peaks (in red) and valleys (in deep blue) which could be problematic for obtaining a dense and gastight electrolyte film, and b) a smoother LSTN surface with a mean roughness of ~2.6 µm without sharp peaks more suitable for successful PLD deposition. Reducing the solid content from 29 to 22 wt% together with reduced spray flow allowed fabrication of sufficiently smooth layers. After optimization, the samples present a good coverage and good adhesion to the metal support with a thickness of 30 to 40 µm. LSTN forms a uniform, nanoporous layer with grain size < 500 nm favourable for PLD as depicted by the cross section images in Figure 7.

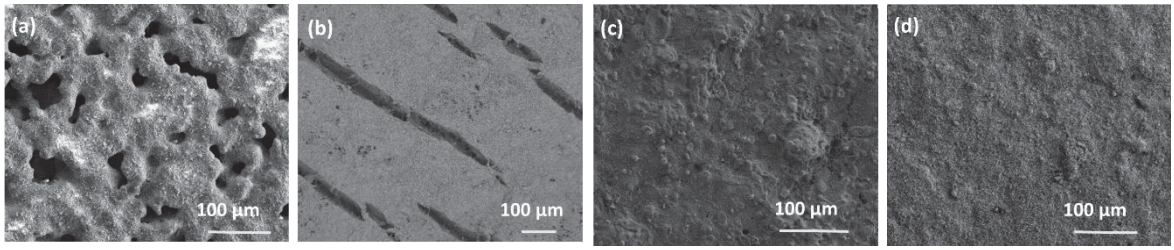

Figure 5 SEM surface micrographs of LSTN spray-coated layers on metal support presenting the improvement of the LSTN deposition. (a) – (b) show large holes and cracks on a LSTN layer obtained with a 37 wt% concentrated suspension directly sprayed on a MS with low and high flow respectively; (c) – (d) show the effect of the squeeged LSTN layer and the reduction of suspension concentration and flow rate.

Table 1 Spray-coating parameters used to illustrate the adjustement performed to obtain LSTN buffer layer with suitable surface for PLD deposition. (* Weight including both squeeged and spray-coated layer)

LSTN solid content (wt%)	Squeegee LSTN layer	Number of depositons × Spray flow ($ml.min^{-1}$)	LSTN weight per surface area after sintering* ($g.cm^{-2}$)	Observation after sintering
37	-	5 × 1	0.0288	Warped support - many cracks, unstable spray - Fig.5b
37	-	1 × 0.75 + 2 × 0.5	0.0099	Large holes from MS, unstable spray – Fig. 5a
29	Yes	2 × 0.75 + 1 × 0.5	0.0107	Flat support but rough surface – Fig.5c and Fig.6a
22	Yes	5 × 0.5	0.0073	Nice surface, some remaining holes Fig.5d
22	Yes	5 × 0.75	0.0145	Nice and smooth surface - 30

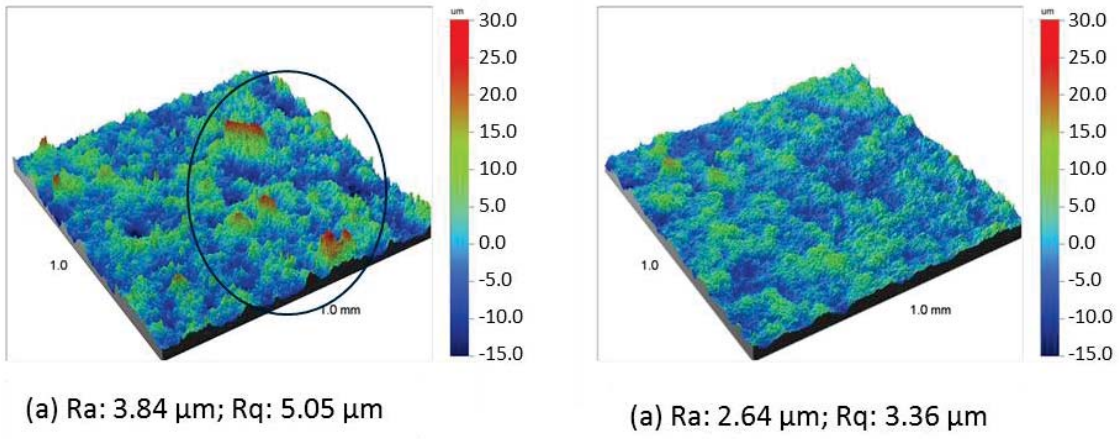

Figure 6 WLI image of two different LSTN spray-coated layers at a magnification of 27 times over an evaluation area of 1 × 1 mm^2. (Ra = Roughness average is the main height as calculated over the entire measured area, and Rq = Root means square (rms) is the average between the height deviations and the mean surface, taken over the evaluation area.)

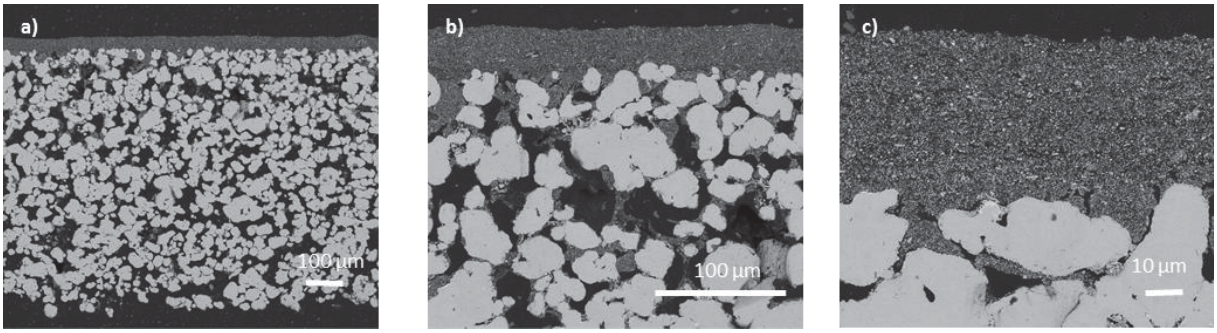

Figure 7 SEM cross-section micrographs of LSTN spray-coated layers on metal support after sintering in H_2/Ar at 1160 °C.

PLD of cathode and electrolyte layers: BZY15–NiO cathode and BZY15 electrolyte were deposited on MS/LSTN samples that had a surface roughness of ~1–3 µm. The thin BZY15–NiO and BZY15 films were obtained as separate films, with different microstructures by applying different deposition conditions. The cathode was deposited at 700 °C and the electrolyte was deposited at lower temperature, 600 °C, in order to avoid sintering of the two

layers into one densified single layer (Figure 8). The O_2 pressure during the depositions was gradually reduced from 0.25 mbar to 0.02 mbar to promote a gradual transition from porous to dense layer. The procedure also reduced the strain in the two layers thereby avoiding delamination of the deposited layers. The deposition conditions summarized in Table 2 lead to a columnar unreduced cathode with some porosity and a dense electrolyte as shown in Figure 8. Both surface and cross-section micrographs show a good densification of the BZY15 electrolyte, without any visible stress-induced cracks. In a previous work, we deposited the BZY15–NiO cathode at 800 °C [23], while here we were able to reduce the cathode deposition temperature to 700 °C for a better preservation of the metal support in the oxygen-containing low-pressure atmosphere. As will be shown later, the electrode porosity was increased after reduction of NiO to Ni.

X-ray diffractograms of BZY15 films deposited at 600 °C and 0.02 mbar O_2 were collected in grazing angle mode (GI-XRD) and confirmed the formation of single phase, crystalline films without significant crystallographic texture (not shown). More details about PLD depositions of BZY15 and BZY15–NiO on porous metal supports can be found in [23].

Table 2: Deposition conditions for BZY15–NiO and BZY15 films on porous MS/LSTN assemblies.

Material	E (J/cm^2)	F (Hz)	P (mbar)	T (°C)	TSD (cm)	Substrate
BZY–NiO	1.6	7	0.25 – 0.15	700	6	MS/LSTN
BZY	1.6	5	0.10 – 0.02	600	6	

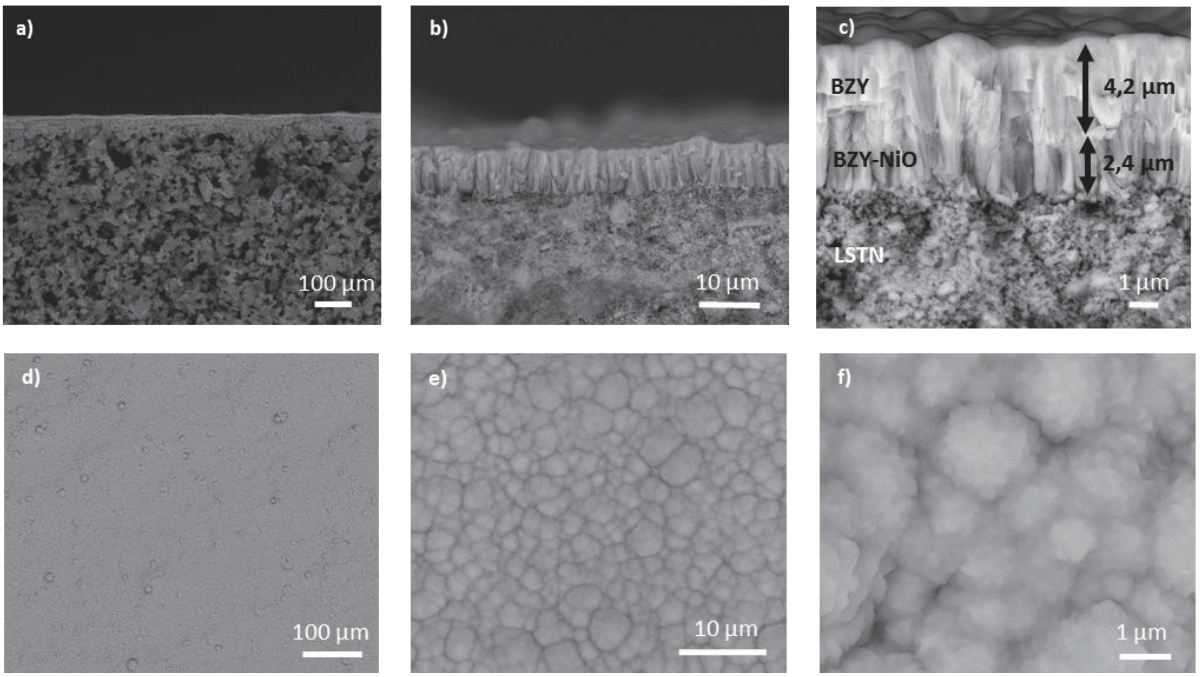

Figure 8 SEM micrographs of BZY15–NiO cathode and BZY15 electrolyte deposited on MS/LSTN substrate (a) – (c) shows the cross section, while (d) – (f) shows the top surface of the BZY15 electrolyte deposited on MS/LSTN/BZY15–NiO.

BZY15–NiO cathode reduction step and initial electrochemical testing: Two half cell assemblies (Table 3) were subjected to reducing conditions (dry H_2/Ar mixture) at temperatures between 400 °C – 650 °C in order to reduce the NiO to Ni and thereby also increasing the porosity of the cathode layer. One cell (cell 2) was tested electrochemically and is described below. The obtained thicknesses of the different functional layers for two half cells are summarized in Table 3.

Table 3. Fabrication conditions and resulting thicknesses for two MS/LSTN/BZY15–Ni/BZY15 half cells.

Cell #	MS sintering T (°C)	MS thickness (µm)	Coating T (°C)	LSTN sintering T (°C)	LSTN thickness (µm)	PLD T (°C)	BZY15 – NiO thickness (µm)	BZY15 thickness (µm)
1	1175	500	900	1160	30	700–600	1	3
2	1175	500	900	1175	20	700–600	3–4	3

Cell 1 was characterized by SEM and with EDS element analysis after reduction (Figure 9). Cross sections (Figure 9 c–e) show that even though the BZY15–NiO deposition was made at lower temperature (700 °C, instead of 800 °C [23]), the NiO was reduced to Ni particles without significant Ni coarsening. The porosity of the BZY15–Ni cathode was increased upon the reduction step, while the BZY15 electrolyte layer retained its columnar, dense structure. The EDS line scan of the cross section of half cell 1 after reduction treatment at temperatures up to 575 °C (Figure 9 f) indicates that Ni interdiffusion from the cathode to the electrolyte cannot be ruled out; however, 750 °C is above the targeted operating temperature of the cell and at lower temperatures the Ni interdiffusion will be slowed down. Since the electron signal from BZY and BZY–Ni comes from an inferference sphere of diamterer ~ 0.5 – 1 µm at 15 kV, and since the sample is not flat, some contributing signal from underlaying BZY–Ni cannot be excluded to be the origin of the small Ni signal from the BZY layer.

As illustrated in Figure 9, there are some porous areas between the LSTN buffer layer and BZY15–Ni electrode which may be less mechanically robust and prone to delamination. The quality of the buffer layer is obviously a critical step in the MS-PCEC fabrication, both in terms of microstructure, conductivity and stability. This matter will be further addressed in future work.

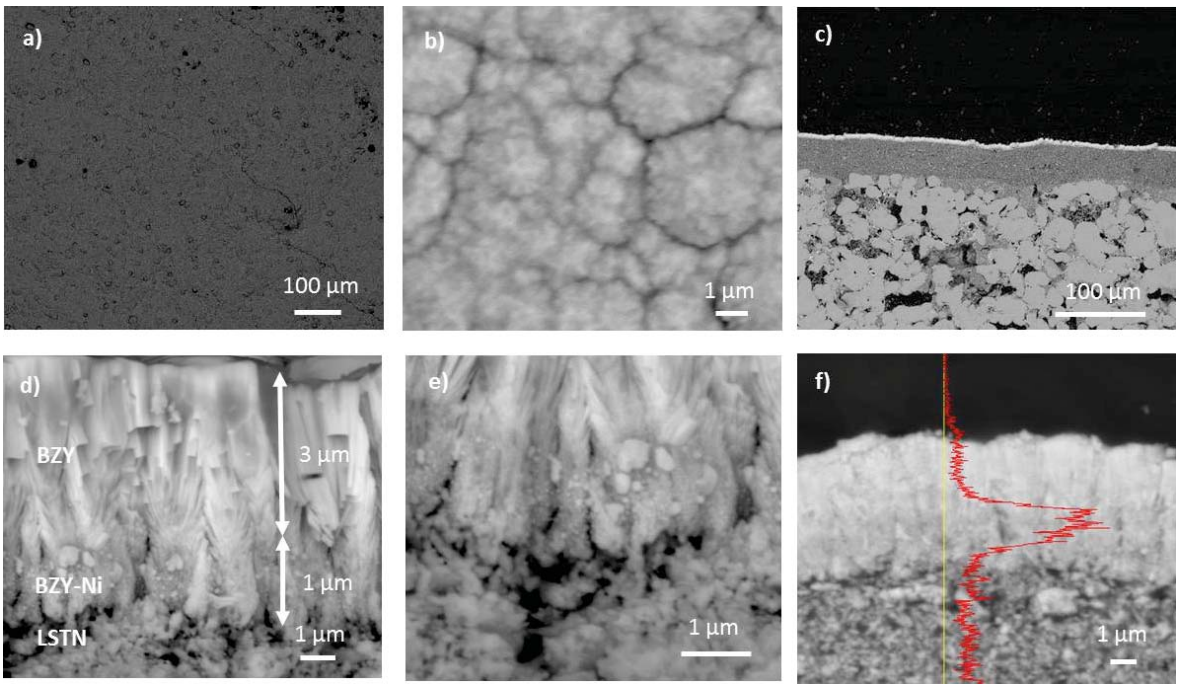

Figure 9. SEM micrographs (15 kV acceleration voltage) of half cells after reduction of BZY–NiO. (a), (b) show the surface of the BZY electrolyte in half cell 1, while (c) – (e) show cross

section images of half cell 1, and (f) shows cross section of half cell 1. In (f) the red line lines mark Ni composition obained by EDS in a line of the cross-section.

Figure 10 shows the total resistance of cell 2 as determined from impedance spectra, after reduction at 450 °C and increasing temperature to 650 °C. The spectra at higher temperatures were dominated by a semicircle with a capacitance of approximately 3×10^{-8} F, which indicates a high grain boundary resistance. The total resistance was 40 $\Omega\cdot cm^2$ at 600 °C which is at least one order of magnitude too high to be used in practical applications. This initial electrochemical testing shows that further optimization of the cell components is required, especially to reduce the grain boundary resistance, for instance by post-annealing after PLD. The procedures for protonation (humidification) and NiO/LSTN reduction also need to be optimized and studied as function of time.

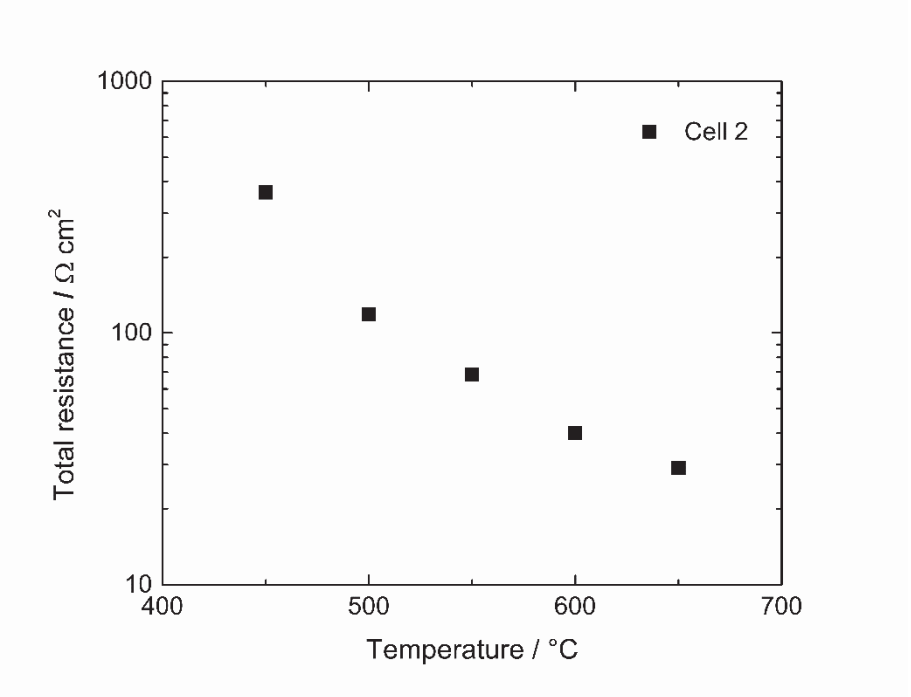

Figure 10. Total resistance of cell 2 with 3% H_2O in Ar on the anode side (Pt) and 100% H_2 on the MS side.

The next step in the development of MS-PCEC is naturally the deposition of an optimized oxide anode (steam electrode) onto the MS/LSTN/BZY15–NiO/BZY15 half cell in order to obtain a full cell with better performance than the Pt-based anode used here. As the deposition or sintering temperature of the oxide anode layer preferably should be ≤ 800 °C to minimize oxidation of the metal support and to maintain the microstructure of the PLD layers, spray-coating of a nanoparticle suspension and PLD are viable methods also for the anode.

4. Conclusions

Important advances have been made in fabrication of planar metal supported PCEC assemblies. The overall procedure follows: i) tape casting of a porous ferritic stainless steel support with tailored microstructure, ii) application of a protective coating to decrease the oxidation of the steel during fabrication and testing, iii) spray coating of an buffer LSTN oxide layer to decreased the roughness of the metal substrate, iv) deposition of BZY15–NiO electrode and BZY15 electrolyte films by PLD.

Metal support sintering temperature have been optimised to obtain sufficent mechanical strength for cathode and electrolyte deposition. The oxidation resistance of the metal supports, both in air and wet H_2/Ar at 600 and 700 °C was significantly reduced after application of the protective coating. The solid content of the suspension together with the flow parameters, the number of sprayed layers, as well as post annealing processes of the LSTN layer have been optimized. The PLD of BZY15–Ni electrode and BZY15 proton conducting electrolyte films were sequentially deposited on metal supports at elevated substrate temperatures and resulted in crystalline porous BZY15–NiO and dense BZY15 films. These different microstructures for the electrode and the electrolyte were achieved in one process with deposition at different substrate temperatures (700 °C for the electrode and 600 °C for the electrolyte) and a gradual decrease of the ambient pressure followed by reduction of NiO to Ni to increase the porosity in the cathode resulting in the desired MS/LSTN/(BZY15–Ni)/BZY15 layered half cell structure. Initial electrochemical testing with a Pt anode showed a total resistance of 40 $\Omega \cdot cm^2$ at 600 °C, when using gas flows of 3% H_2O in Ar at the anode side and 100% H_2 on the cathode side. Cell fabrication and testing is still ongoing with focus on optimising the buffer layer as well as deposition of the steam electrode.

Acknowledgements

The financial support from the Research Council of Norway, via the METALLICA project, grant agreement 221819/E20 is greatly acknowledged.

References

[1] Brisse A, Schefold J, Stoots C, O'Brien J. Chapter 9:Electrolysis Using Fuel Cell Technology. Chapter 9Electrolysis Using Fuel Cell Technol., 2010, p. 263–86.
[2] Goñi-Urtiaga A, Presvytes D, Scott K. Solid acids as electrolyte materials for proton exchange membrane (PEM) electrolysis: Review. Int J Hydrog Energy 2012;37:3358–72. doi:10.1016/j.ijhydene.2011.09.152.
[3] Ferrero D, Lanzini A, Santarelli M, Leone P. A comparative assessment on hydrogen production from low- and high-temperature electrolysis. Int J Hydrog Energy 2013;38:3523–36. doi:10.1016/j.ijhydene.2013.01.065.
[4] Ni M, Leung M, Leung D. Technological development of hydrogen production by solid oxide electrolyzer cell (SOEC). Int J Hydrog Energy 2008;33:2337–54. doi:10.1016/j.ijhydene.2008.02.048.
[5] Schiller G, Ansar A, Lang M, Patz O. High temperature water electrolysis using metal supported solid oxide electrolyser cells (SOEC). J Appl Electrochem 2009;39:293–301.
[6] Bi L, Boulfrad S, Traversa E. Steam electrolysis by solid oxide electrolysis cells (SOECs) with proton-conducting oxides. Chem Soc Rev 2014;43:8255–70. doi:10.1039/C4CS00194J.
[7] Blennow P, Hjelm J, Klemensø T, Persson A, Brodersen K, Srivastava A, et al. Development of Planar Metal Supported SOFC with Novel Cermet Anode. ECS Trans 2009;25:701–10. doi:10.1149/1.3205585.
[8] Pham H-C, Park E-J, Taniguchi S, Sasaki K. Development of a Porous Metal Substrate for Metal Supported SOFCs Using a Fe-Cr-Al Stainless Steel. ECS Trans 2013;57:2289–93. doi:10.1149/05701.2289ecst.
[9] Fabbri E, D'Epifanio A, Di Bartolomeo E, Licoccia S, Traversa E. Tailoring the chemical stability of Ba(Ce0.8 − xZrx)Y0.2O3 − δ protonic conductors for Intermediate Temperature Solid Oxide Fuel Cells (IT-SOFCs). Solid State Ion 2008;179:558–64. doi:10.1016/j.ssi.2008.04.002.
[10] Kreuer KD. Aspects of the formation and mobility of protonic charge carriers and the stability of perovskite-type oxides. Solid State Ion 1999;125:285–302. doi:10.1016/S0167-2738(99)00188-5.
[11] Pergolesi D, Fabbri E, Traversa E. Chemically stable anode-supported solid oxide fuel cells based on Y-doped barium zirconate thin films having improved performance. Electrochem Commun 2010;12:977–80. doi:10.1016/j.elecom.2010.05.005.
[12] Bae K, Jang DY, Choi HJ, Kim D, Hong J, Kim B-K, et al. Demonstrating the potential of yttrium-doped barium zirconate electrolyte for high-performance fuel cells. Nat Commun 2017;8:14553. doi:10.1038/ncomms14553.
[13] Tong J, Clark D, Bernau L, Sanders M, O'Hayre R. Solid-state reactive sintering mechanism for large-grained yttrium-doped barium zirconate proton conducting ceramics. J Mater Chem 2010;20:6333–41. doi:10.1039/C0JM00381F.
[14] Nielsen J, Klemensø T, Blennow P. Detailed impedance characterization of a well performing and durable Ni:CGO infiltrated cermet anode for metal-supported solid oxide fuel cells. J Power Sources 2012;219:305–16. doi:10.1016/j.jpowsour.2012.07.031.
[15] Thornton JA. Influence of apparatus geometry and deposition conditions on the structure and topography of thick sputtered coatings. J Vac Sci Technol 1974;11:666–70. doi:10.1116/1.1312732.
[16] Evans A, Bieberle-Hütter A, Rupp JLM, Gauckler LJ. Review on microfabricated micro-solid oxide fuel cell membranes. J Power Sources 2009;194:119–29. doi:10.1016/j.jpowsour.2009.03.048.

[17] Evans A, Martynczuk J, Stender D, Schneider CW, Lippert T, Prestat M. Low-Temperature Micro-Solid Oxide Fuel Cells with Partially Amorphous La0.6Sr0.4CoO3-δ Cathodes. Adv Energy Mater 2015;5:n/a-n/a. doi:10.1002/aenm.201400747.
[18] Ishihara T, Eto H, Yan J. Intermediate temperature solid oxide fuel cells using LaGaO3 based oxide film deposited by PLD method. Int J Hydrog Energy 2011;36:1862–7. doi:10.1016/j.ijhydene.2009.12.174.
[19] Noh H-S, Park J-S, Son J-W, Lee H, Lee J-H, Lee H-W. Physical and Microstructural Properties of NiO- and Ni-YSZ Composite Thin Films Fabricated by Pulsed-Laser Deposition at T≤700°C. J Am Ceram Soc 2009;92:3059–64. doi:10.1111/j.1551-2916.2009.03362.x.
[20] Noh H-S, Son J-W, Lee H, Ji H-I, Lee J-H, Lee H-W. Suppression of Ni agglomeration in PLD fabricated Ni-YSZ composite for surface modification of SOFC anode. J Eur Ceram Soc 2010;30:3415–23. doi:10.1016/j.jeurceramsoc.2010.07.035.
[21] Noh H-S, Yoon KJ, Kim B-K, Je H-J, Lee H-W, Lee J-H, et al. The potential and challenges of thin-film electrolyte and nanostructured electrode for yttria-stabilized zirconia-base anode-supported solid oxide fuel cells. J Power Sources 2014;247:105–11. doi:10.1016/j.jpowsour.2013.08.072.
[22] Blank DHA, Dekkers M, Rijnders G. Pulsed laser deposition in Twente: from research tool towards industrial deposition. J Phys Appl Phys 2014;47:034006. doi:10.1088/0022-3727/47/3/034006.
[23] Stefan E, Stange M, Denonville C, Larring Y, Haugsrud R, Hildenbrand N, et al. Layered Microstructures based on BaZr0.85Y0.15O3-δ by Pulsed Laser Deposition for Metal Supported Proton Ceramic Electrolyzer Cells. J Mater Chem A n.d.
[24] Arrivé C, Delahaye T, Joubert O, Gauthier G. Exsolution of nickel nanoparticles at the surface of a conducting titanate as potential hydrogen electrode material for solid oxide electrochemical cells. J Power Sources 2013;223:341–8. doi:10.1016/j.jpowsour.2012.09.062.
[25] Tsekouras G, Neagu D, Irvine JTS. Step-change in high temperature steam electrolysis performance of perovskite oxide cathodes with exsolution of B-site dopants. Energy Environ Sci 2012;6:256–66. doi:10.1039/C2EE22547F.
[26] Stange M, Denonville C, Larring Y, Haavik C, Brevet A, Montani A, et al. Coating Developments for Metal-Supported Solid Oxide Fuel Cells. ECS Trans 2013;57:511–20. doi:10.1149/05701.0511ecst.